Time-gated luminescence bioimaging with new luminescent nanocolloids based on [Mo6I8(C2F5COO)(6)](2-) metal atom clusters

Chrystelle Neaime, Maria Amela-Cortes, Fabien Grasset, Yann Molard, Stéphane Cordier, Benjamin Dierre, Michel Mortier, Toshiaki Takei, Kohsei Takahashi, Hajime Haneda, et al.

Time-Gated Luminescence Bioimaging with new Luminescent Nanocolloids based on $[Mo_6I_8(C_2F_5COO)_6]^{2-}$ Metal Atom Clusters

Chrystelle Neaime[a], Maria Amela-Cortes[a] Fabien Grasset[a,b*], Yann Molard[a], Stéphane Cordier[a*], Benjamin Dierre[b], Michel Mortier[c], Toshiaki Takei[d], Kohsei Takahashi[e], Hajime Haneda[e], Marc Verelst[f] and Séverine Lechevallier[f*]

Bioimaging and cell labeling using red or near infrared phosphors emitting in the "therapeutic window" of biological tissues have recently become one of the most active research fields in modern medical diagnostic. However, because organic and inorganic autofluorophores are omnipresent in nature, very often background signal from fluorochromes other than targeted probes have to be eliminated. This discrimination could be available using a time-gated luminescence microscopy (TGLM) technique associated with long lifetime phosphorescent nanocomposites. Here, we report new SiO_2 nanostructured particles (50 nm in diameter) embbeded luminescent nanosized $[Mo_6I_8(C_2F_5COO)_6]^{2-}$ metal atom clusters (1 nm in diameter), succesfully prepared by the microemulsion technique. This combination provides new physical insight and displays red emission in biological based solution under UV-Vis excitation with long lifetimes around 17 and 84 µs. Moreover, the nanoparticles can be internalized by cancer cells after surface functionalization by transferrin protein and clearly imaged by TGLM under excitation at 365 nm. The nanocomposite have been mainly characterized by scanning and transmission electron microscopies (SEM and HAADF-STEM), UV-Vis and photoluminescence (PL) spectroscopies.

1-Introduction

Biomedical imaging and cell labelling using red or near infrared (NIR) phosphors emitting in the so-called “therapeutic window” of biological tissue (600-900 nm) have recently become one of the most active research fields in modern medical diagnostic.[1,2] However, because organic and inorganic autofluorophores are omnipresent in nature, very often the background signal from fluorochromes other than targeted probes or the autofluorescence under UV-visible excitation have to be eliminated.[1] This discrimination could be available using (i) NIR excitation source (ii) a time-resolved fluorescence microscopy (TRFM) technique operating in the frequency domain or (iii) a time-gated luminescence microscopy (TGLM) technique operating in the time domain.[1,3] The latter appears to be simpler and much less costly than the others. Indeed, building such a microscope is quite easy and does not require expensive furnitures (for example the acquisition system is a simple camera). Nevertheless, time-gated luminescence (TGL) detection requires that targeted organisms are labelled with a long-lived luminescent probe, typically with a luminescence lifetime > 50-100 µs, more than 500 times the common biological autofluorescence lifetimes (τ < 100 ns). Generally, complex organic dyes, silicon nanoparticles, lanthanide chelates or lanthanide doped nanocrystals fluorescent probes with long lifetime (close to milliseconds for some compounds) are used.[4-8] Nevertheless, our reliance on rare-earth minerals and the consequently environmental problems due to their extraction encourage us to a strong development of new contrast agents nanomaterials.[9]

Concerning nanophosphors doped silica nanoparticles, they have been the subject of continuous scientific interests since the 90s owing to their important applications in biological fluorescence labelling thanks to their wide band gap, cost-effectiveness and biocompatibility.[10-12] Functional silica nanoparticles with magnetic and/or optical properties have attracted much attention for numerous applications not only in the fields of biotechnologies but also photonics.[13,14] They are usually achieved through the encapsulation of superparamagnetic nanocrystals such as ferrites[15] or photonic nanocrystals such as metal nanoparticles[16,17] or luminescent nanophosphors such as organic dyes,[18,19] semi-conductor quantum dots,[20-27] organometallic complexes,[28,29] metal atom cluster (MC)[30-34] or doped nanocrystals.[35-37] Thus, since 2006, some of us developed a simple, versatile, highly reproducible and efficient method based on microemulsion process to prepare large amount of silica nanoparticles incorporating luminescent nanosized inorganic Mo_6 or Re_6 metal atom clusters based on octahedra.[30-34] These MC salts are generally synthesized by a solid state chemistry route at high

[a] CNRS-UR1, UMR 6226, Institut des Sciences Chimiques de Rennes (ISCR), Université de Rennes 1, Campus de Beaulieu, 35042 Rennes Cedex, France Email : fabien.grasset@univ-rennes1.fr
[b] CNRS-Saint Gobain-NIMS, UMI 3629, Laboratory for Innovative Key Materials and Structures–LINK, National Institute of Material Science (NIMS), 1-1 Namiki, 305-0044, Tsukuba, Japan
[c] Chimie ParisTech, PSL Research University, CNRS, Institut de Recherche de Chimie Paris, 75005 Paris, France
[d] International Center for Materials Nanoarchitectonics, MANA, National Institute of Material Science, 1-1 Namiki, Tsukuba 305-0044, Japan
[e] National Institute of Material Science, 1-1 Namiki, Tsukuba 305-0044, Japan
[f] CHROMALYS, 29 rue Jeanne Marvig, 31400 Toulouse

† Footnotes relating to the title and/or authors should appear here.
Electronic Supplementary Information (ESI) available: [details of any supplementary information available should be included here]. See DOI: 10.1039/x0xx00000x

$_8X\ ]^{2-}$ nano-sized cluster units (M = Mo, W or Re) wherein the M_6 cluster is face-capped by eight inner ligands (X^i) and additionally bonded to six apical ligands (X^a). Owing to the ionic nature of the interaction between the cluster units and the counter-cations (K^+, Cs^+, tetrabutylammonium…), the solid state powder can be dispersed at nanosized level in solution.[30] Even after high dispersion in organic or inorganic matrix, Mo_6 or Re_6 metal atom clusters exhibit a characteristic broad emission band in the red and NIR (550–900 nm),[30,34,40] which is particularly interesting for biotechnology applications as it corresponds to a low human tissues absorption at these wavelengths. Moreover, some of these MC could generate singlet oxygen under irradiation, which is of particular interest for photodynamic therapy (PDT) applications.[41,42] Thus, all these works already have demonstrated that Mo_6 or Re_6 cluster units may represent a complementary alternative to traditional luminophores (organic dyes, QDs or lanthanide based nanocrystals) developed for theranostic applications. In this work, we describe the preparation and the application of a new contrast agent for TGL for biological applications. A highly luminescent metal atom cluster unit with high quantum yield was used as phosphor and we demonstrate the one-pot preparation of monodispersed $Cs_2Mo_6I_8(C_2F_5COO)_6$@SiO_2 nanostructured particles by using a simple microemulsion process. In a second time, human transferrin (Tf) was conjugated on the surface of silica nanoparticles, following a three steps protocol, to enhance the cellular uptake. Although transferrin has been already applied to enhance cellular uptake of functional silica nanoparticles,[43,44] the present study is, to the best of our knowledge, the first report on the preparation of transferrin grafted silica nanoparticles loaded by metal atom clusters used for TGL observation.

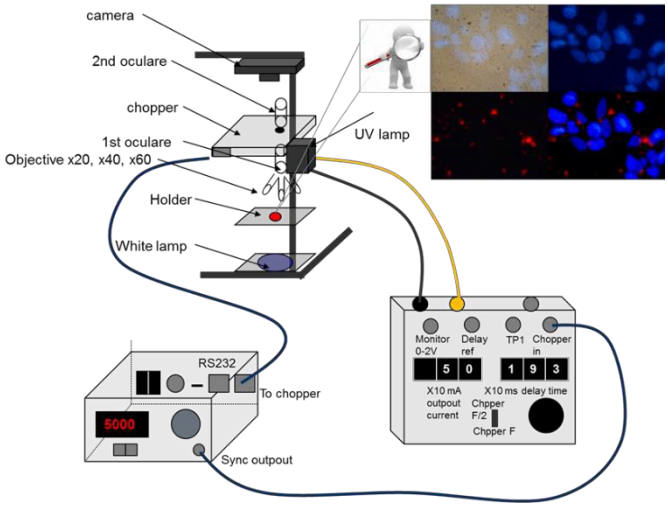

Fig. 1. Schematic view of TGLM set-up.

2-Experimental details

2-1. Structural, physico-chemical and optical characterization

Field emission scanning electron microscopy (FE-SEM) images were taken using an ultra-high resolution scanning electron microscope Hitachi SU8000 with cold cathode field emission source. Bright-field transmission electron microscopy (TEM) images were taken using a Cs-corrected JEOL 2100F microscope operating at 200 kV. It is equipped with a field-emission electron gun and incorporates multiple additional functions such as an energy-dispersive spectrometry (EDS) and a high-sensitivity Z-contrast high angular annular dark field scanning transmission electron microscopy (HAADF-STEM) analysis. Sample was prepared by direct deposition of powder dispersed in CCl_4 on carbon-activated copper grids. Zeta potential were measured by using a Nanosizer ZS Malvern Instrument (λ=630 nm), considering viscosity and refraction index of water. Photoluminescence (PL) measurements were done with a Horiba-Jobin-Yvon Fluorolog lll fluorescence spectrometer with a Xe lamp. The luminescence spectra were recorded at room temperature in quartz cuvette (0,01mg/L). The data were collected at every nm with an integration time of 100 ms for each step. Absolute quantum yield was measured in colloidal solution with a Hamamatsu C9920-03G system. Time-resolved photoluminescence measurements were performed on powder at room temperature in quartz tube with a device using an intensified charge-coupled device (ICCD) PI-Max camera placed at the exit slit of a 0.30 m Acton Research Corporation monochromator. 6 ns excitation pulses were provided by an optical parametric oscillator (OPO) optically pumped by the third harmonic of a Nd:YAG Q-switched laser. Time-gated luminescence microscopy has been realized under excitation wavelength of 365 nm using a "home-made" microscope kindly built for us by Dr Dayong Jin from Macquarie University of Sydney (Figure 1). All the luminescence measurements have been done in presence of O_2.

2-2. Raw materials

Polyoxyethylene (4) lauryl ether (Brij® L4), tetraethoxysilane (TEOS, 99%), (3-aminopropyl)triethoxysilane (APTES, 99%), human transferrin (Tf), 1-ethyl-3-(3-dimethylaminopropyl)carbodiimide (EDAC), 2-(N-Morpholino)ethanesulfonic acid hydrate, 4-morpholineethanesulfonic acid (MES, >99.5%), anhydrous dimethylformamide (DMF), Phosphate-buffered saline (PBS), 4',6-diamidino-2-phénylindole (DAPI); acetonitrile, glycine, succinic anhydride and silver pentafluoropropionate were purchased from Sigma-Aldrich. Ammonia (28 wt % in water) and n-heptane (99%) were purchased from VWR. Ethanol (99.80%) was purchased from Fluka.

2-3. Preparation of $Cs_2Mo_6I_8(C_2F_5COO)_6$ MC

The $Cs_2Mo_6I_8(C_2F_5COO)_6$ cluster compound was prepared from $Cs_2Mo_6I^i_8\,{}^a_6$ and $AgOCOC_2F_5$ (See SI for detailed experimental procedure) The compound integrity and purity were confirmed by ^{19}F-NMR (acetone d_6) with the presence of only two signals at δ = -83 ppm and δ = -120 ppm, by EDS and X-ray diffraction on single crystals. All data were in agreement with previously published results.[45]

2-4. Preparation of $Cs_2Mo_6I_8(C_2F_5COO)_6$@SiO_2 nanocolloids

The functional silica nanoparticles have been prepared using a water-in-oil (W/O) microemulsion process developed by our group since the earlier 2000[15, 30, 32, 33]. Typically, 47 mL of heptane (oil-phase) was mixed with 15 mL of surfactant (Brij® L4). Then is added successively a complex aqueous cluster solution [$Cs_2Mo_6I_8(C_2F_5COO)_6$]=0.025 mol/L (1.6 mL) and finally an aqueous ammonia solution (28%, 1.3 mL). The precursor of silica (TEOS, 2 mL) was added one hour later. After the addition of TEOS, the solution is stirred for 72 h and then the microemulsion is destabilized with ethanol. Same conditions

were used to prepare $Cs_2Mo_6I_{14}@SiO_2$ for optical properties comparison. Finally, the nanoparticles were collected and washed once with ethanol by centrifuging at 20000 G during 20 minutes and then five times with water in order to remove the surfactant molecules (40000 G during at least 30 minutes) before being dispersed in purified water at concentration around 10 g/L. Previous experiments on $[Mo_6Br_{14}]^{2-}$ clusters have demonstrated that similar colloid is stable several weeks with an absence of leakage of MC after encapsulation into silica[32].

2-5. Preparation of Tf-conjugated $Cs_2Mo_6I_8(C_2F_5COO)_6@SiO_2$ nanocolloid

$Cs_2Mo_6I_8(C_2F_5COO)_6@SiO_2$ nanoparticles have been conjugated with transferrin following a three steps protocol. First, the silica nanoparticle have been functionalized with APTES in order to obtain amino-modified nanoparticles. Typically, 36.5 mg of $Cs_2Mo_6I_8(C_2F_5COO)_6@SiO_2$ nanocolloids are suspended in 11 mL acetonitrile and sonicated in an ultrasonic bath. Then 182 µL of APTES are added drop wise and the suspension is stirred at 50°C for 24h. Finally nanoparticles are collected by centrifugation and washed three times with ethanol and water. In a second step, as-grafted amino groups have been converted into carboxyl functions using succinic anhydride (20 mg per mg of nanocolloids) in DMF under inert atmosphere. Finally, carboxyl-modified nanoparticles have been conjugated with transferrin following a protocol described by Pitek et al.[46] 10 mg of carboxyl-modified colloids have been suspended in 5 mL of MES buffer. Then 5 mg of transferrin dissolved in 5 mL of MES have been added to the suspension. After stirring at 37°C for 10 min, 10 mg of EDAC were added and the reaction was continued for 2h. To stop the reaction, 20 mg of glycine were added and the Tf-conjugated nanoparticles were collected by centrifugation (15 min, 3260 G), washed three times with PBS and dried under vacuum at room temperature. Surface potential has been measured after each step: naked: Z=-31.4 mV, amino-modified: Z=+4.3 mV, carboxyl-modified: Z=+0.1 mV, Tf-modified: Z=-18 mV. Transferrin has also been quantified by UV-Vis spectroscopy. It has been found a concentration of 0.27 mg of Tf by mg of nanoparticle.

2-6. Cell culture and cellular uptake

SKmel 28 cell lines of human melanoma have been cultivated in RPMI 1640 medium with 10% of fetal bovine serum (FBS) at 37°C with 5% of CO_2. Practically, cells have been seeded in 96-well plates at a concentration between 50000 cells by point in 500 µL of culture medium for fluorescence experimentations and 10000 cells by point in 200 µL of culture medium for inductively coupled plasma (ICP) experimentations. Next day, the culture medium is replaced with the same culture medium containing the Tf-nanoparticles at a concentration of 0.1 mg/mL. Cells have been incubated with the nanoparticles for 1, 2, 8 and 24h. For each condition, experiments have been repeated 4 times for fluorescence and 9 times for ICP. After incubation, culture medium containing the nanocolloids was removed, and cells have been washed 2 times with PBS. For fluorescence experimentations cells were mounted with a mounting medium containing DAPI (Vectashield H1500). Mounting medium has been added in order to color nuclei of the cells. It is also usually used to reduce the photo blinking of DAPI. For ICP experimentations cells were detached with trypsine and dissolved in 5 mL of NaOH 1N (Sigma-Aldrich). Same experiment were performed with nanoparticles without conjugated Tf and these nanoparticles were not internalized.

3-Results and discussion

3-1. Structure and morphology of $Cs_2Mo_6I_8(C_2F_5COO)_6@SiO_2$ nanoparticles

Microemulsions are thermodynamically stable dispersions of two immiscible fluids (i.e. n-heptane and complex water phase) stabilized by the arrangement of surfactant molecules (i.e. Brij® L4) at the interface.[47] The water in oil (W/O) microemulsions consist of nanodroplets of complex water phase dispersed in an oil phase and stabilized in spherical reverse micelles created by the surfactant molecules.

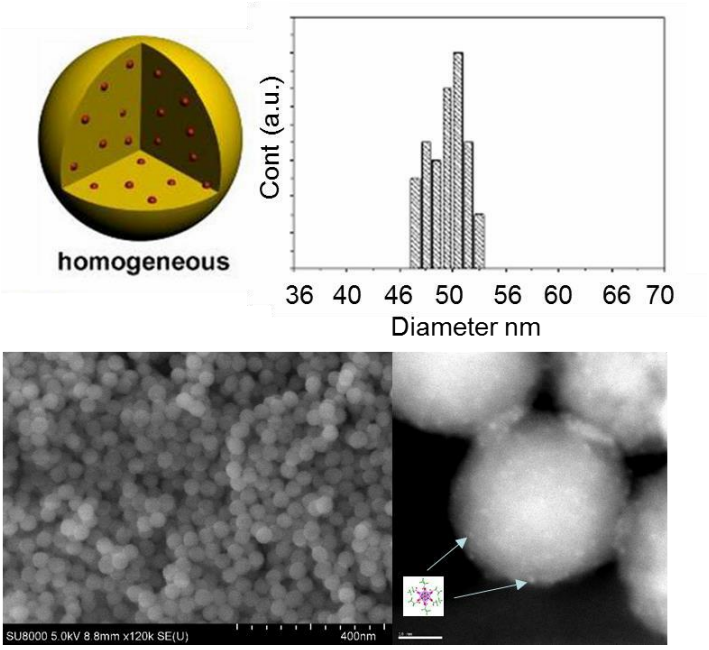

Fig. 2. Schematic homogeneous nanoparticle (top left). SEM (bottom left, bar is 400 nm) and HAADF-STEM (bottom right, bar is 10 nm) images of $Cs_2Mo_6I_8(C_2F_5COO)_6@SiO_2$ and histogram of the diameter (top right).

Those hydrophilic droplets can then be considered as "nanoreactors" and by controlling the molar ratio of the mixture oil/water/surfactant, it is possible to predetermine the size of those droplets (in the range of few tens nanometers) and, as a consequence, to tailor the size of the final silica nanoparticles. By using microemulsion sol-gel processes, it was recently demonstrated that several complex architecture of functional silica nanoparticles could be obtained.[48,49] In detail, the complex water phase was prepared by dissolving the $Cs_2Mo_6I_8(C_2F_5COO)_6$ cluster compound in a mixture of ethanol and distilled water (1:1 volume ratio). Based on our previous works on $Cs_2Mo_6Br_{14}@SiO_2$ nanoparticles, the concentration of the CMIF cluster solution was fixed to 0.025 M.[32] Thanks to this W/O microemulsion process, the Mo_6 cluster units were efficiently encapsulated in the silica nanoparticles with a good stability and reproducibility even with negative charge. A typical SEM and HAADF-STEM images of the $Cs_2Mo_6I_8(C_2F_5COO)_6@SiO_2$ nanoparticles are shown in **Figure 2**. The nanoparticles present the so-called homogenous architectur[20] (Fig. 2 top left) and are relatively monodispersed in size. The techniques showed that the silica nanoparticles consisted of an arrangement of

relatively uniform particles with an average particle diameter of 50 nm (Fig. 2 bottom left). Thanks to the HAADF-STEM mode image in high resolution (Fig. 2 bottom right), it is clearly possible to observe the Mo_6 units inside the @SiO_2 nanoparticles. As it can be observed in figure 2 (bottom right), the cluster units, represented by light spots of ca. 1 nm diameter, are relatively well dispersed inside and at the surface of the silica nanoparticle. Similar results were observed for $Cs_2Mo_6I_{14}$@SiO_2 nanoparticles. The Mo/Si atomic ratio is estimated at 0.01 for $Cs_2Mo_6I_8(C_2F_5COO)_6$@SiO_2 and 0.006 for $Cs_2Mo_6I_{14}$@SiO_2 by EDS analysis. Nevertheless, even if I and F have been detected by EDS, this technique is not accurate to give a chemical composition due a too high dilution of these 3 elements and low stability of sample under e-beam irradiation.

3-2. Optical properties of $Cs_2Mo_6I_8(C_2F_5COO)_6$@SiO_2 nanoparticles

The successful encapsulation of the $Cs_2Mo_6I_8(C_2F_5COO)_6$ cluster compound in the silica nanoparticles was mainly evidenced by the spectroscopic investigations of the luminescence properties of $Cs_2Mo_6I_8(C_2F_5COO)_6$@SiO_2 nanocolloids. As phosphor dyes, the luminescence of clusters is quenched by interaction with solubilized molecular oxygen.[32,45] Indeed without any protection layer (silica or polymer) Mo_6 cluster cannot emit in water phase. This behavior is explained by the excitation of triplet oxygen from excited triplet states of the cluster to form singlet oxygen.[50] This point was also demonstrated with Mo_6 or Re_6 clusters by using bubbling O_2 and/or Ar atmosphere.[31-33] As we can see on **Figure 3**, this quenching effect was successfully limited by embedding the cluster units in silica nanoparticles, and a clear red luminescence could be observed with eyes under UV irradiation at 365 nm.

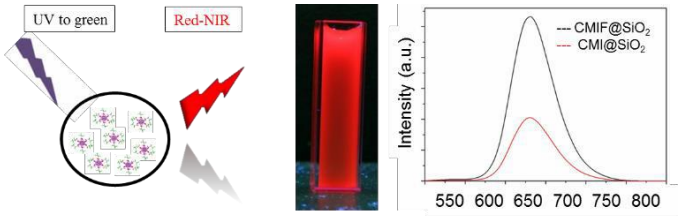

Fig. 3. Sketch of excitation and emission of functional nanoparticles (left), photograph of $Cs_2Mo_6I_8(C_2F_5COO)_6$@SiO_2 nanocolloid in aqueous solution (10 g/l) under UV (365 nm) irradiation (middle) and emission spectra of the of $Cs_2Mo_6I_8(C_2F_5COO)_6$@SiO_2 and $Cs_2Mo_6I_{14}$@SiO_2 nanocolloids at 0,01 g/l (right).

The luminescence properties of the $Cs_2Mo_6I_8(C_2F_5COO)_6$@SiO_2 nanocolloids were compared to those of the $Cs_2Mo_6I_{14}$@SiO_2 dispersed in aqueous media. The same concentration of clusters and similar condition experiments were used in order to compare the intensity of both colloidal solutions. The obtained emission spectra are gathered in figure 3 and it is clear that the intensity of the colloidal solution containing the highly luminescent $Cs_2Mo_6I_8(C_2F_5COO)_6$ cluster[45] compound is three time higher than for those containing $Cs_2Mo_6I_{14}$. This result is explained by a better solubility of the fluorinated clusters into silica matrix (see Mo/Si ratio above) maybe due to favorable H-bonding formation[32] and/or a better luminescence efficiency of fluorinated clusters as reported by Kirakci et al. for similar compounds.[52] The maximum of luminescence centered at 655 nm is in good agreement with previous results obtained for polymer containing the $Cs_2Mo_6I_8(C_2F_5COO)_6$ cluster.[45] In the case of $Cs_2Mo_6I_{14}$ clusters, to explain the maximum centered at 657 nm, we have to consider that iodide apical ligands could be exchanged by OH groups in aqueous solution during the microemulsion process due to the HSAB principle.[50] Indeed, the difference between photo-luminescence properties of $Cs_2Mo_6I^i_8I^a_6$ solid state compound and those of $Cs_2Mo_6I^i_8I^a_6$@SiO_2 is due to the substitution of apical iodides by OH groups that influence the nature of excited states and consequently the de-excitation pathways. This classically induces a shift of emission maxima. Similar findings were already observed in the case of bromide homologous. Indeed, the encapsulation of $Cs_2Mo_6Br_{14}$ or $Cs_4[Re_6S_8Br_6]$ in silica nanoparticles results in the substitution of apical bromine atoms by OH groups and as a consequence in a shift of the emission maximum of the clusters roughly equal to 70 nm to lower wavelengths.[31, 32]

The internal quantum yield of the colloidal solution containing $Cs_2Mo_6I_8(C_2F_5COO)_6$@SiO_2 was estimated at 0.03. Phosphorescence decay profiles, which are the key parameter for TGLM, were studied using wavelength of 700 nm with an excitation wavelength at 400 nm. Lifetime of powder and colloidal containing clusters embedded in the @SiO_2 nanoparticles results are summarized in Table 1. Phosphorescence decay profiles were fitted to a two-exponential decay with long and short lifetime components. Lifetimes were calculated with one around 17 µs and one around 84 µs. These values are perfectly suitable for TGL experiments and are in good accordance with reported lifetimes values for $Cs_2Mo_6I_8(C_2F_5COO)_6$ powder (91 µs) or after encapsulation in polymer (13 µs and 70 µs).[45]

	Lifetime 1 (A1)	Lifetime 2 (A2)
Powder	17 µs (0.51)	84 µs (0.49)
Colloidal solution	13 µs (0.90)	70 µs (0.1)

Table 1: Lifetime of powder and colloidal solution. The kinetic parameters were obtained by fitting the luminescence decay curves with a three exponential equation as followed: $y = A1e(-x/\tau1) + A2e(-x/\tau2) + y_0$. A1 and A2 represent the ponderation coefficient of each exponential.

The mechanisms of de-excitation of the clusters are complex leading to a multicomponent emission[51]. They depend on the natures of (i) the metal, (ii) inner ligands and (iii) apical ligands. Moreover, it is sensitive to the nature of counter cations. Concerning $Mo_6I^i_8L^a_6$ cluster units (L = carboxylate group), the recent joint work of Kitamura and Sokolov[51] evidences that photo-luminescent properties depend more on pKa than on the length of ligand. The longer lifetimes of $Cs_2Mo_6I^i_8(OOCC^2F^5)^a_6$ compared to $Cs^2Mo^6I^i_8I^a_6$ are mainly attributed to different excited states owing to the different natures of apical ligands and consequently to evolution of molecular orbital energy levels. Indeed, the similar lifetimes of $Cs_2Mo_6I_8(OOCC_2F_5)_6$ and $Cs_2Mo_6I_8(OOCC_2F_5)_6$@SiO_2 (i) confirm that no apical ligands exchanges occur during the encapsulation process and (ii) that electronic interactions between $[Mo_6I_8(OOCC_2F_5)_6]^{2-}$ cluster units and the silica matrix are poor.

3-3. TGLM experiment and cellular uptake of Tf-conjugated $Cs_2Mo_6I_8(C_2F_5COO)_6@SiO_2$ nanocolloids.

3-3-1 TGML observation of labelled cells

As described in the introduction part, the main interest of a TGLM is to be able to separate long lasting fluorescence coming from Mo_6 clusters and the auto fluorescence coming from the biological media. These properties are evidenced on **Figure 4**, which presents images of the Tf-nanoparticles internalized by cancer cells, recorded with the different modes of the TGLM. On the images, nuclei colored with DAPI appear in blue, and Tf-nanoparticles in red. Images are in true colors. Under UV irradiation and without delay, only cells nuclei are visible (Figure 4a and b). With a delay, the red luminescence of the Tf-nanoparticles is clearly observed, whereas all the fluorescence coming from the DAPI and the surrounding medium is clearly extinguished (Figure 4c). The figure 4d is the merge of the two modes, and allows to localize the NPs inside the cells.

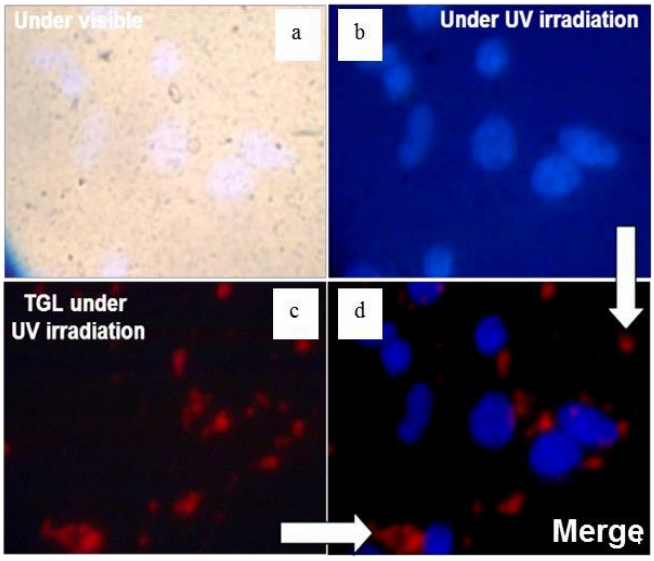

Fig. 4: Images of the Tf-nanoparticles internalized by cancer cells using different modes of the time-gated luminescence microscope, under excitation at 365 nm: a) bright field, b) direct (without delay), c) time gated (delay≈10 µs), d) is the merge of b and c.

Moreover, cells incubated with the Tf-conjugated $Cs_2Mo_6I_8(C_2F_5COO)_6@SiO_2$ nanoparticles for various times have been observed with TGLM (Fig. 5). Images show again clearly the presence of red spots around the nuclei, characteristics of the nanoparticles. However, depending on the incubation times, the density of these spots varies. Thus, for incubation time of 1 or 2h, cells present a relatively strong perinuclear red luminescence indicating a good internalization of the Tf-nanoparticles into the cytoplasm and a good labelling. For longer incubation times (8h), the labelling is weaker and finally vanished after 24h.

3-3-2 Quantitative analysis

In order to quantify the internalization of the Tf-nanoparticles by the cell, the concentration of molybdenum has been determined by ICP after incubation of the cells with the Tf-nanoparticles. Results are presented in Table 2. The quantities of molybdenum measured inside cells (between 1.4 and 1.9 pg of Mo per cell) are weak and reach quickly a plateau.

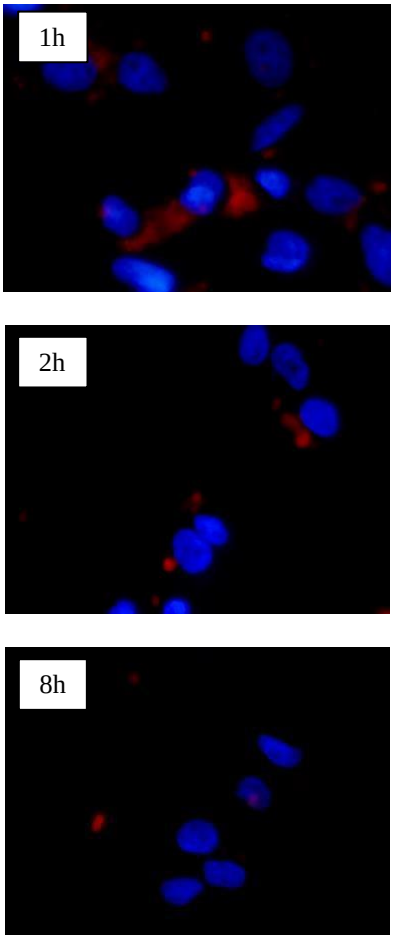

Fig. 5: Merged images of "direct" and "time gated" mode of SKmel 28 cells incubated with Tf-conjugated nanoparticles for various times (1h, 2h or 8h), under excitation at 365 nm.

This point could be related to the important cellular death for long incubation times (8 and 24h). For incubation time of 1h, the values are consistent with the observations realized by luminescence microscopy: the significant but heterogeneous labelling of the cells. For incubation times of 8h and 24h, still living cells are probably those having little or no internalized nanoparticles.

Incubation time	[Mo] mg/L	[Mo] mg/5mL	[Mo] pg/cell
1h	0.025	0.00013	1.44
8h	0.031	0.00016	1.78
24h	0.033	0.00017	1.89

Table 2: Results of ICP quantification of Mo internalized in cells for various times

Indeed, after 8 and 24h of incubation, living cells exhibit only very few particles in their cytoplasm. For quantitative analysis by ICP, the observed cellular toxicity probably induced a bias because ICP does not discriminate living and dead cells. Nevertheless, the disappearance of labelling, due to cellular death, increases with incubation time, which may indicate a cellular toxicity of the nanoparticles for this type of cancer cells. Although it is not the aim of this study, this toxicity could be explained in a first approximation by the production of reactive oxygen species (ROS) under UV excitation at the surface of the silica Tf-nanoparticles, where clusters can interact with molecular oxygen. Indeed, the trifluoroacetate family cluster compounds is reported to have a high rate of singlet-oxygen formation.[51, 52] These points should be improved and further investigated. This toxicity could be suppressed or at least strongly reduced by adding a silica layer by seed-growth process at the surface of the nanoparticles. Moreover, the toxicity of nanomaterials depends also of cell lines[53] and more, of the model of cell cultures targeted. For instance, Re_6 octahedral cluster coated with polymer were internalized into human cervical adenocarcinoma HeLa cells, in particular, mainly localized in the cytoplasm and nucleus without acute cytotoxicity whereas pure Mo_6 clusters greatly inhibited plant growth (without affected seed germination)[53] and this inhibition was totally suppressed after coated by silica.[53] The selection of appropriate cell line for use in mechanistic-based studies remains a critical component in nanotoxicology. This point was again recently pointed out by studying the toxicity of functional silica nanoparticles containing $Cs_2Mo_6Br_{14}$ clusters on three types of cells (A549, L929 and KB). The cell viability was measured by MTT test in monolayer culture whereas the cytotoxicity in spheroid 3D model was examined by the APH assay.[53] The main results showed that human KB carcinoma cells are very sensitive to functional @SiO_2 nanoparticles unlike both A549 and L929 cell lines did not exhibit susceptibility.

Conclusions

This work reports on the preparation, structural and optical properties of new luminescent nanocomposite silica nanoparticles for biotechnology applications. This new nanomaterial is based on the homogenous encapsulation into silica nanoparticles of luminescent $[Mo_6I_8(C_2F_5COO)_6]^{2-}$ phosphors containing Mo_6 metal atom clusters by the microemulsion technique. The as-prepared $Cs_2Mo_6I_8(C_2F_5COO)_6$@SiO_2 nanoparticles have a perfect spherical shape with a good monodispersity. The size of the dispersed cluster and silica nanoparticles matrix are 1 and 50 nm in diameter, respectively. This nanocomposite displays a red emission in biological based solution under UV-Vis excitation. The calculated lifetimes are around 17 and 84 µs, which fit perfectly with TGML requirements. It was demonstrated that the nanoparticles can be internalized by cancer cells after surface functionalization by transferrin protein and imaged by time-gated luminescence microscopy under excitation at 365 nm. The main interest of a TGLM is to separate long lasting fluorescence coming from Mo_6 clusters and the auto fluorescence coming from the biological media. Consequently, they seem to be well adapted for *in vitro* imaging on cell cultures and TGL flow cytometry devices.[54] Although, a full toxicity study is needed to go further, these results seem to be relevant for future applications of functional silica nanoparticles based on metal atom clusters in bionanotechnology.

Acknowledgements

The manuscript was written through contributions of all authors. All authors have given approval to the final version of the manuscript. These works have been financially supported by the University of Rennes 1, the CNRS, NIMS-MANA and ANR (CLUSTOP-11-BS08-013-01).

Notes and references

1 L. Chu, S. Wang, K. Li, W. Xi, X. Zhao, J. Qian, *Biomed Opt Express.*, 2014, **5(11)**, 4076-4088
2 K. Ariga, Q. Ji, M.J. McShane, Y.M. Lvov, A. Vinu, J.P. Hill, *Chem. Mater.*, 2012, **24(5)**, 728–737
3 R. Connally, D. Jin, J. Piper, *Cytometry. Part A,* 2006, **69A**, 1020-1027
4 N. Gahlaut, L. W. Miller, *Cytometry Part A,* 2010, **77A**, 1113–1125 ; J. Dayong, P.A. James, *Anal. Chem.*, 2011, **83(6)**, 2294-2300
5 L. Gu, D.J. Hall, Z. Qin, E. Anglin, J. Joo, D. J. Mooney, S. B. Howell, M. J. Sailor, *Nat. Commun.,* 2013, 4, 2326 ; MJ.S. Chandra, B. Ghosh, G. Beaune, U. Nagarajan, T. Yasui, J. Nakamura, T. Tsuruoka, Y. Baba, N. Shirahata, F. M. Winnik, *Nanoscale*, 2016, **8**, 9009–9019
6 S.A. Osseni, S. Lechevallier, M. Verelst, P. Perriat, J. Dexpert-Ghys, D. Neumeyer, R. Garcia, F. Mayer, K. Djanashvili, J.A. Peters, E. Magdeleine, H. Gros-Dagnac, P. Celsis, R. Mauricot, *Nanoscale*, 2014, **6**, 555–564 ; L. Zhang, X. Zheng, W. Deng, Y. Lu, S. Lechevallier, Z. Ye, E.M. Goldys, J.M. Dawes, J.A. Piper, J. Yuan, M. Verelst, D. Jin, *Sci. Rep.*, 2014, **4**, 6597 ; J.A Zhou, N. Shirahata, H.-T. Sun, B. Ghosh, M. Ogawara, Y. Teng, S. Zhou, R. G. S. Chu, M. Fujii, J. Qiu. *J. Phys. Chem. Lett.,* 2013, **4**, 402−408
7 Z. Chen, K. Y. Zhang, X. Tong, Y. Liu, C. Hu, S. Liu, Qi Yu, Q. Zhao, W. Huang, *Adv. Funct. Mater.,* 2016, **26**, 4386–4396 ; W. Lv, T. Yang, Q. Yu, Q. Zhao, K. Y. Zhang, H. Liang, S. Liu, F. Li, W. Huang, Adv. Sci. 2015, 2, 1500107 ; H. Sun, J. Zhang, K. Y. Zhang, S. Liu, H. Liang, W. Lv ,W.i Qiao, X. Liu, T. Yang, Q. Zhao, W. Huang, *Part. Part. Syst. Charact.,* 2015, **32**, 48–53 ; Q. Zhao, X. Zhou, T. Cao, K. Y. Zhang, L. Yang, S. Liu, H. Liang, H. Yang, F. Li, W. Huang, *Chem. Sci.*, 2015, **6**, 1825–1831
8 A. Vaasa, K. Ligi, S. Mohandessi, E. Enkvist, A. Uri, L.W. Miller, *Chem. Commun.*, 2012, **48**, 8595–8597
9 A.R. Jha, Rare Earth Materials: Properties and Applications, CRC Press, 2014

10 A. Burns, J. Vider, H. Ow, E. Herz, O. Penate-Medina, M. Baumgart, S.M. Larson, U. Wiesner, M. Bradbury, *Nano Lett.,* 2009, **9**, 442-448.
11 J.L. Vivero-Escoto, R.C. Huxford-Phillips, W. Lin, *Chem. Soc. Rev.,* 2012, **41**, 2673-2685.
12 Y. Kuthati, P.J. Sung, C.F. Weng, C.Y. Mou, C.H. Lee, *J. Nanosci. Nanotech.,* 2013, **13(4)**, 2399-2430.
13 M.A. Noginov, G. Zhu, A.M. Belgrave, R. Bakker, V.M. Shalaev, E.E. Narimanov, S. Stout, E. Herz, T. Suteewong, U. Wiesner, *Nature,* 2009, **460**, 1110-1112.
14 J.F. Dechézelles, T. Aubert, F. Grasset, S. Cordier, C. Barthou, C. Schwob, A. Maitre, R.A.L. Vallée, H. Cramail, S. Ravaine, *Phys. Chem. Chem. Phys.,* 2010, **12**, 11993-11999.
15 F. Grasset, N. Labhsetwar, D. Li, D.C. Park, N. Saito, H. Haneda, O. Cador, T. Roisnel, S. Mornet, E. Duguet, J. Portier, J. Etourneau, *Langmuir,* 2002, **18**, 8209-8216.
16 L.M. Liz-Marzan, M. Giersig, P. Mulvaney, *Langmuir,* 1996, **12**, 4329-4335.
17 J.H. Son, H.Y. Park, D.P. Kang, D.S. Bae, *Colloids Surf. A: Physicochem. Eng. Aspects,* 2008, **313–314**, 105–107.
18 A. Van Blaaderen, A. Vrij, *Langmuir,* 1992, **8**, 2921-2931.
19 H. Ow, D.R. Larson, M. Srivastava, B.A. Baird, W.W. Webb, U. Wiesner, *Nano Lett.,* 2005, **5**, 113-117.
20 S.Y. Chang, L. Liu, S.A. Asher, *J. Am. Chem. Soc.,* 1994, **116**, 6739-6744.
21 P. Mulvaney, L.M. Liz-Marzan, M. Giersig, T. Ung, *J. Mater. Chem.,* 2000, **10**, 1259-1270.
22 D. Gerion, F. Pinaud, S.C. Williams, W.J. Parak, D. Zanchet, S. Weiss, A.P. Alivisatos, *J. Phys. Chem. B,* 2001, **105**, 8861-8871.
23 J. Lovrić, H.S. Bazzi, Y. Cuie, G.R. Fortin, F.M. Winnik, D. Maysinger, *J. Mol. Med.,* 2005, **83(5)**, 377-385.
24 T. Aubert, S.J. Soenen, D. Wassmuth, M. Cirillo, R.V. Deun, K. Braeckmans, Z. Hens, *ACS Appl Mater Interfaces,* 2014, **6(14)**, 11714-11723.
25 X. Tang, E.S.G. Choo, L. Li, J. Xue, *Chem. Mater.,* 2010, **22**, 3383-3388.
26 H.J. Zhang, H.M. Xiong, Q.G. Ren, Y.Y. Xia, J.L. Kong, *J. Mater. Chem.*, 2012, **22**, 13159-13165.
27 K. Matsuyama, N. Ihsan, K. Irie, K. Mishima, T. Okuyama, H. Muto, *J. Colloid Interface Sci.,* 2013, **399**, 19-25.
28 S. Santra, P. Zhang, K. Wang, R. Tapec, W. Tan, *Anal. Chem.,* 2001, **73**, 4988-4993.
29 R.P. Bagwe, C. Yang, L.R. Hilliard, W. Tan, *Langmuir,* 2004, **20**, 8336-8342.
30 F. Grasset, F. Dorson, S. Cordier, Y. Molard, C. Perrin, A.M. Marie, T. Sasaki, H. Haneda, Y. Bando, M. Mortier, *Adv. Mater.,* 2008, **20**, 143-148 ; S. Cordier, F. Dorson, F. Grasset, Y. Molard, B. Fabre, H. Haneda, T. Sasaki, M. Mortier, S. Ababou-Girard, C. Perrin, *J. Clust. Sci.*, 2009, **20(1)**, 9-21.
31 T. Aubert, A. Y. Ledneva, F. Grasset, K. Kimoto, N. G. Naumov, Y. Molard, N. Saito, H. Haneda, S. Cordier, *Langmuir,* 2010, **26(23)**, 18512–18518
32 T. Aubert, F. Cabello Hurtado, M.A. Esnault, C. Neaime, D. Lebret-Chauvel, S. Jeanne, P. Pellen, C. Roiland, L. Le Polles, N. Saito, K. Kimoto, H. Haneda, N. Ohashi, F. Grasset, S. Cordier, *J. Phys. Chem. C,* 2013, **117**, 20154–20163.
33 N. Nerambourg, T. Aubert, C. Neaime, S. Cordier, M. Mortier, G. Patriarche, F. Grasset, *J. Colloid Interface Sci.,* 2014, **424**, 132–140.
34 A.O. Solovieva, Y.A. Vorotnikov, K.E. Trifonova, O.A. Efremova, A.A. Krasilnikova, K.A. Brylev, E.V. Vorontsova, P.A. Avrorov, L.V. Shestopalova, A.F. Poveshchenko, Y.V. Mironov, M.A. Shestopalov, J. *Mater. Chem. B,* 2016, 4, 4839-4846
35 Z. Li, Y. Zhang, *Angew. Chem. Int. Ed.* 2006, **45**, 7732-7735.
36 S. Nagarajan, Z. Li, V. Marchi-Artzner, F. Grasset, Y. Zhang, *Med. Biol. Eng. Comput.,* 2010, **48**, 1033-1041.
37 H.T. Sun, J. Yang, M. Fujii, Y. Sakka, Y. Zhu, T. Asahara, N. Shirahata, M. Li, Z. Bai, J.G. Li, H. Gao, *Small,* 2011, **7**, 199-203.
38 A. Perrin, C. Perrin, *C. R. Chimie,* 2012, **15**, 815–836.
39 V. Fedorov, *J. Clust. Sci.*, 2015, **26**, 3-15
40 S. Cordier, Y. Molard, K.A. Brylev, Y.V. Mironov, F. Grasset, B. Fabre, N.G. Naumov, *J. Cluster. Sci.,* 2015, **26**, 53-81.
41 L. Gao, M.A. Peay, T.G. Gray, *Chem. Mater.,* 2010, **22**, 6240-6245.
42 K. Kirakci, P. Kubát, K. Fejfarová, J. Martinčík, M. Nikl, K. Lang, *Inorg. Chem.*, 2016, **55(2)**, 803-809.
43 Y. Cui, Q. Xu, P.K.H. Chow, D. Wang, C.H. Wang, *Biomaterials* 2013, **34**, 8511-8520.
44 D.P. Ferris, J. Lu, C. Gothard, R. Yanes, C.R. Thomas, J.C. Olsen, J.F. Stoddart, F. Tamanoi, J.I. Zink, *Small*, 2011, **7(13)**, 1816-1926
45 M. Amela-Cortes, S. Paofai, S. Cordier, H. Folliot, Y. Molard, *Chem. Commun.* 2015, **51**, 8177-8180 ; T. G. Truong, B. Dierre, F. Grasset, N. Saito, N. Saito, T. K. N. Nguyen, K. Takahashi, T. Uchikoshi, M. Amela-Cortes, Y. Molard, S. Cordier, N. Ohashi, *Sci. Technol. Adv. Mat.* 2016, **17(1)**, 443-453 ; M. Amela-Cortes, Y. Molard, S. Paofai, A. Desert, J.-L. Duvail, N.G. Naumov, S. Cordier, *Dalton Trans*., 2016, **45**, 237-245 ; K. Kirakci, S. Cordier, C. Perrin, *Z. Anorg. Allg. Chem.*, 2005, **631**, 411-416 ; N. Huby, J. Bigeon, Q. Lagneaux, M. Amela-Cortes, A. Garreau, Y. Molard, J. Fade, A. Desert, E. Faulques, B. Bêche, J.L. Duvail, S. Cordier, *Opt. Mater.*, 2016, 52, 196-202
46 A.S. Pitek, D. O'Connell, E. Mahon, M.P. Monopoli, F.B. Bombelli, K.A. Dawson, *PLoS One,* 2012, **7(7)**, e40685.
47 M.A. Lopez-Quintela, *Curr. Opin. Colloid Interface Sci.*, 2003, **8**, 137-144
48 T. Aubert, F. Grasset, S. Mornet, E. Duguet, O. Cador, S. Cordier, Y. Molard, V. Demange, M. Mortier, H. Haneda, *J. Colloid Interface Sci.,* 2010, **341**, 201-208.
49 J. Wang, Z.H. Shah, S. Zhang, R. Lu, *Nanoscale*, 2014, **6**, 4418-4437
50 L. Riehl, M. Ströbele, D. Enseling, T. Jüstel, H.J. Meyer, *Z. Anorg. Allg. Chem.,* 2016, **642(5)**, 403–407
51 K. Costuas, A. Garreau, A. Bulou, B. Fontaine, J. Cuny, R. Gautier, M. Mortier, Y. Molard, J.-L. Duvail, E. Faulques, S. Cordier, *Phys. Chem. Chem. Phys*., 2015, **17**, 28574-28585 ; M. A. Mikhailov, K. A. Brylev, P. A. Abramov, E. Sakuda, S. Akagi, A. Ito, N. Kitamura, M. N. Sokolov, Inorg. Chem., 2016, 55, 8437−8445
52 K. Kirakci, P. Kubát, J. Langmaier, T. Polívka, M. Fuciman, K. Fejfarovád, K. Lang, *Dalton Trans.*, 2013, **42**, 7224–7232 ; A. Beltran, M. Mikhailov, M. N. Sokolov, V. Perez-Laguna, A. Rezusta, M.J. Revillo, F. Galindo, *J. Mater. Chem. B*, 2016, 4, 5975-5979
53 S. J. Choi, K. A. Brylev, J.-Z. Xu, Y. V. Mironov, V. E. Fedorov, Y. S Sohn, S. J. Kim, J.-H. Choy, *J. Inorg. Biochem.*, 2008, **102**, 1991-1996; T. Aubert, A. Burel, M.-A. Esnault, S. Cordier, F. Grasset, F. Cabello-Hurtado, *J. Hazard. Mater.*, 2012, **219–220**, 111– 118 ; F. Cabello-Hurtado. M. D. Lozano-Baena. C. Neaime. A. Burel. S. Jeanne, P. Pellen-Mussi, S. Cordier. F. Grasset, *J. Nanopart. Res.*, 2016, **18**, 69-84 ; A. Godard, S. Tricot-Doleux, P. Pellen-Mussi, C. Neaime, N. Nerambourg, F. Cabello-Hurtado, S. Cordier, F. Grasset, S. Jeanne, *J. Nanopart. Res.*, submitted
54 D. Jin, R. Connally, J. Piper, *Cytometry Part A,* 2007, **71A**, 783-796 ; D. Jin, R. Connally, J. Piper, *Cytometry Part A,* 2007, **71A**, 797-808